Crystal structure and f-orbital hybridization in the filled skutterudite $PrRu_4P_{12}$

Jonathan Buhot,[1,2,3,*] Marie-Bernadette Lepetit,[4,5] Hitoshi Sugawara,[6] and Marie-Aude Méasson[1,7,†]
[1]*Laboratoire Matériaux et Phénomènes Quantiques, UMR 7162 CNRS, Université Paris Diderot, Bât. Condorcet 75205 Paris Cedex 13, France*
[2]*High Field Magnet Laboratory (HFML - EMFL), Radboud University, 6525 ED Nijmegen, The Netherlands*
[3]*HH Wills Laboratory, University of Bristol, Bristol BS8 1TL, United Kingdom*
[4]*Univ. Grenoble Alpes, CNRS, Grenoble INP, Institut Néel, 38000 Grenoble, France*
[5]*Institut Laue Langevin, 38000 Grenoble, France*
[6]*Department of Physics, Kobe University, Kobe 657-85301 Japan*
[7]*Univ. Grenoble Alpes, CNRS, Grenoble INP, Institut Néel, 38000 Grenoble, France*

(Received 29 March 2023; accepted 18 September 2023; published 20 October 2023)

The lattice dynamic of the filled skutterudite $PrRu_4P_{12}$ has been investigated by both Raman spectroscopy and density-functional theory (DFT) calculations, through the metal to insulator transition at 63 K. A $P23$ space group, which lacks inversion symmetry, is identified for the low temperature phase. The classical room-temperature $Im\bar{3}$ structure reported in the filled skutterudite family is questioned in this compound. Our results point to the $Pm\bar{3}$ space group, which already has two distinct Pr sites in the metallic state at room temperature. The consequences of symmetry breaking, between $Pm\bar{3}$ and $P23$ on both the f orbital hybridization and the crystal schemes are discussed.

DOI: 10.1103/PhysRevMaterials.7.105001

I. INTRODUCTION

Skutterudite materials have attracted a lot of attention for their good thermoelectric performance [1], as well as for their fundamental properties [2]. Indeed, filled skutterudites of general formula RT_4X_{12} (where R is a lanthaninde or actinide, T a transition metal, and X a pnictogen) exhibit a wide variety of quantum phenomena [2–4], such as unconventional superconductivity [5], heavy fermions states [6], antiferromagnetic order [7], and multipolar orders [8,9]. Both the hybridization of the f electron with the conduction electrons and the crystal electric field effects on the rare-earth orbital degrees of freedom [2,10] are the key ingredients responsible for such zoology of quantum phases and their interactions.

This is specifically the case in the $PrRu_4P_{12}$ compound, where a metal-to-insulator (MI) transition occurs at 63 K and is associated with a change in the crystal electric field levels behavior [11–13]. A differentiation of the crystal electric field scheme of the two rare-earth sites is reported at the transition [12], and a recent RIXS study [14] confirmed a spatial modulation, related to the two distinct Pr sites in the structure, of the orbital hybridization between Pr $4f$ and P $3p$ in the low temperature phase. The Ru $4d$ electronic states were measured to have much less contribution to the low-temperature phase. Theoretically, this p-f hybridization is expected to stabilize the Γ_4 crystal-field state on one of the Pr at low temperature, while the other Pr site keeps the Γ_1 ground state [10]. Whilst important ingredients of the quantum transition are identified, the nature of the low-temperature quantum ordering remains unclear. In order to solve the question of the nature of this quantum order in $PrRu_4P_{12}$, and more generally in view of studying complex phase transitions driven by crystal-field effects, the determination of the crystal-field scheme as a function of the control parameters (T, P, H) is essential. To do so, one must identify the local point group of the rare-earth site, which involves resolving the exact crystal structure and its associated space group.

From x-ray and electron diffraction, and EXAFS measurements [11,15–19], whereas the high temperature structure has been retained to be $Im\bar{3}$, the structure in the low temperature phase still remains an open question. The authors reported either $Pm\bar{3}$ or $P23$ as good candidates but then selected $Pm\bar{3}$ because of its higher symmetry. Whilst x-ray and electron diffraction measurements are amongst the go-to techniques to determine crystal structures, small crystal distortion (under the instrumental resolution) may remain elusive and thus make impossible to determine a unique space group.

In this paper, thanks to the combination of polarized Raman scattering measurements of the phonon modes in $PrRu_4P_{12}$ and first principle density-functional theory (DFT) calculations, we clarify the space groups of $PrRu_4P_{12}$ above and below the metal-to-insulator transition. The space group of the low temperature phase is identified to be $P23$, one of the candidates proposed by previous diffraction studies. In contrast to what was previously claimed [11], the space group at room temperature is found to be $Pm\bar{3}$ rather than $Im\bar{3}$. The main consequence is that the crystal electric field schemes of the two Pr sites is not degenerated by symmetry in either phases. In the low temperature phase, contrary to the previously suggested space group $Pm\bar{3}$, P23 does not possess

*Jonathan.buhot@bristol.ac.uk
†marie-aude.measson@neel.cnrs.fr

an inversion center. The consequences on the hybridization of the one-electron $4f$ orbitals and their extension is discussed.

II. METHODS

A. Experimental Methods

Two single crystals of $PrRu_4P_{12}$ were prepared by the Sn-flux method. The raw materials were 4N 99.99% pure-La, -Pr, -Ru, 6N-P, and 5N-Sn. An x-ray powder-diffraction experiment confirmed the filled skutterudite structure and absence of any impurity phases [20]. As-grown surface oriented perpendicular to [0,$\bar{1}$,0] and [1,1,1] with high optical quality were directly used for Raman spectroscopy experiments.

Polarized Raman scattering has been performed in quasi-back scattering geometry with an incident laser line at 532 nm from a solid state laser. We used a closed-cycle ^{4}He cryostat for the measurements from 3 K to 300 K. We have estimated the laser heating of the samples at +0.5 K/mW. All temperatures are corrected from laser heating effect. The scattered light was analysed by a Jobin Yvon T64000 triple subtractive grating spectrometer equipped with a cooled CCD detector. The contribution of the Bose factor has been removed for all spectra.

In the following, we will consider the space groups $Im\bar{3}$, $Pm\bar{3}$, and $P23$. The first two groups correspond to the T_h point group with the Raman tensors A_g, ^1E_g, ^2E_g, and T_g, and the latter to the T point group with the Raman tensors A, ^{1}E, ^{2}E, and T. However, the irreducible representations of the Raman tensors A_g and A (respectively, ^1E_g and ^{1}E, ^2E_g and ^{2}E, and T_g and T) are identical which means that the Raman selections rules are the same within both T_h and T point groups. In the $P23$ space group, the irreducible representations are changed from A_g, E_g, and T_g to A, E, and T, respectively. The Raman response was measured in different configurations, namely b(a, a)$\bar{b}$, b(a, c)$\bar{b}$, b(ac, $\bar{a}$c)$\bar{b}$, and b(ac, ac)$\bar{b}$ in the Porto notation, which probe the symmetries $[A_g + E_g]$, $[T_g]$, $[E_g]$, and $[A_g + E_g + T_g]$, respectively.

The local point groups of the Pr atoms, relevant for the crystal electric field excitations symmetries, are T_h for the $Im\bar{3}$ and $Pm\bar{3}$ space groups, and T for $P23$.

B. DFT calculations

The phonons spectra were computed after full geometry optimization in the $Im\bar{3}$, $Pm\bar{3}$, and $P23$ space groups, as well as other $Im\bar{3}$ subgroups that could have been potential candidates for the symmetry groups in one of the phases. The calculations were performed within the density-functional theory (DFT), using the CRYSTAL code [21,22]. We used the Perdew-Burke-Ernzerhof functional revised for solids [23], a very dense Pack-Monkhorst grid of 24 × 24 × 24 (resulting in 663 k points for the $Im\bar{3}$ group), and a Gilat grid of 48 × 48 × 48 for the calculation of the density matrix. We used the standard all-electrons triple-zeta POP basis set for the phosphorus atoms [24], Stuttgart scalar relativistic core pseudopotentials ECP28MDF [25] for the Ru atoms, and ECP48MWB [26] for the Pr atoms. The associated basis sets were modified in order to fit solid state calculations requirements (no function more diffuse than 0.06 exponents).

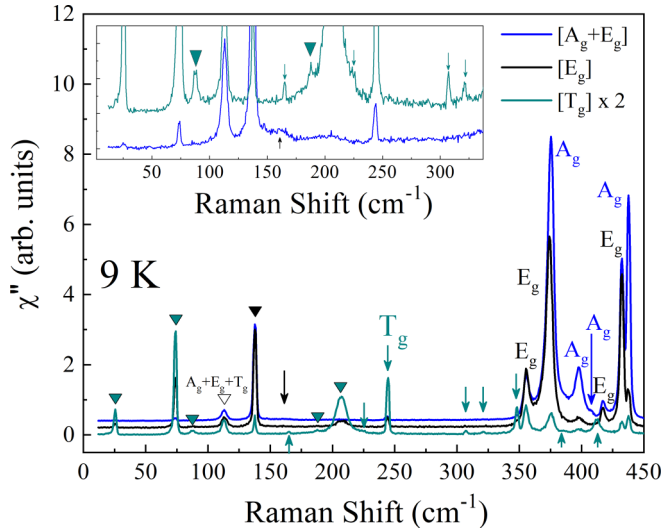

FIG. 1. Raman susceptibility of $PrRu_4P_{12}$ at 9 K in the A_g, E_g, and T_g symmetries. Arrows and triangles point to phonon and crystal-field modes, respectively. Their colors correspond to their symmetries. Inset: zoom on the low-intensity modes.

III. LATTICE DYNAMICS OF THE INSULATING PHASE AT LOW TEMPERATURE

Either $Pm\bar{3}$ or $P23$ space group has been proposed to characterize the crystal structure of $PrRu_4P_{12}$ below $T_{MI} = 60$ K. In this part, by combining vibrational Raman measurements and DFT calculations, we show that the most adequate space group to describe the low temperature crystal structure is $P23$.

Figure 1 presents an overview on the low-temperature Raman modes and their symmetries. A total of 25 modes are measured. The temperature dependencies of the phonon modes for all symmetries are presented in Fig. 2. The structural transition associated with the metal-insulator transition is clearly identified by a change in the phonon spectra below 63 K. Thanks to their temperature dependence, their magnetic

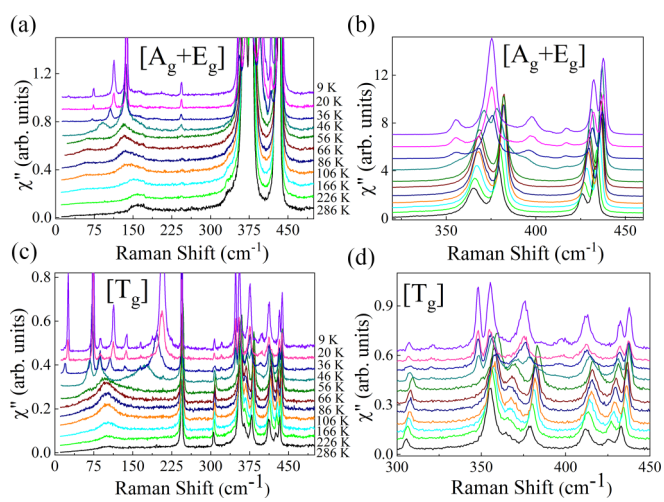

FIG. 2. Raman susceptibility of $PrRu_4P_{12}$ at different temperature down to 9 K. (a) and (b): in the $A_g + E_g$ symmetry. (c) and (d): in the T_g symmetry.

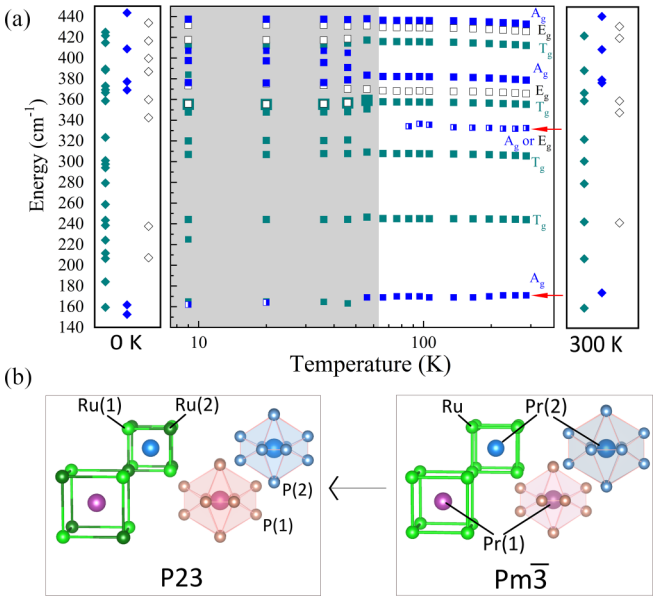

FIG. 3. (a) Energies of the phonon modes of $PrRu_4P_{12}$ versus temperature. Royal blue, black, and green squares are reports of A_g, E_g, and T_g symmetry, respectively. Mixed symmetries are represented by bicolor squares. The gray area highlights the low temperature phase. The red arrows point to the two phonons at 300 K that cannot be attributed in the $Im\bar{3}$ space group. Right and left: calculated modes in the $Pm\bar{3}$ (at 300 K) and $P23$ (at 0 K) space groups, respectively. (b) Illustrations of the Ru- and P-cages transformations through the $Pm\bar{3}$ to $P23$ transition (drawn using VESTA [28]).

field dependence and their pseudovectorlike responses, all the low energy modes below 220 cm^{-1}, except for two modes respectively at 162 and 165 cm^{-1}, are assigned to crystal-field excitations [27]. A total of 18 phonon modes (4 E_g, 9 T_g, 4 A_g, and 1 A_g or E_g at 162 cm^{-1}) is observed at 9 K, while only ten phonon modes are measured at room temperature. Figure 3(a) presents the temperature dependence of the energies of these phonon modes.

Below the metal-to-insulator phase transition at 63 K, EXAFS, x-ray and electron diffraction experiments find the $PrRu_4P_{12}$ compound, either in the $Pm\bar{3}$ or in the $P23$ space groups [16,18,19]. The $Pm\bar{3}$ was preferentially chosen, as it is the most symmetric. However, as mentioned by the authors, tiny distortions leading to the $P23$ space group cannot be excluded.

Therefore, in order to clarify which space group between $Pm\bar{3}$ and $P23$ better describe the crystal structure at low temperature, we have performed geometry optimizations and phonon calculations in both space groups. Then, we have compared these outcomes to our Raman scattering data and to optical conductivity (IR) measurements from Ref. [29]. The geometry optimizations at 0 K yields to nonsignificative differences on the enthalpy and the atomic positions between the two space groups. However, the generalized gradient approximation functionals, such as the PBE (solid) functional we used in the present work, have a tendency to over delocalize the electronic density and thus, over symmetrize the crystal structure. As a consequence, a weak $Pm\bar{3}$ to $P23$ symmetry breaking can be overlooked by such a calculation.

TABLE I. Calculated phonons frequencies in the $Pm\bar{3}$ group at 0 K and assignations with the experimental data in the low temperature phase at 9 K. In bold are the modes with high discrepancy between experiment and calculation results.

Calculations $Pm\bar{3}$ (0 K)		Experiments Raman	IR [29]	Comparison error
Irr. Rep.		ν (cm^{-1})		
Tu	0			
Tu	75.5		75	0.5
Tu	88.9		85	3.9
Tg	132.8			
Ag	151.2	**162**		**10.8**
Tg	159.3	165		5.7
Au	161.9			
Tu	184.0		190	6
Tg	206.9	**225**		**19.1**
Eu	207.1			
Tu	211.9		210	1.9
Tu	224.8		220	4.8
Tu	237.1		230	7.1
Eg	238.1			
Tg	242.9	244		1.1
Tu	258.3		255	3.3
Tg	279.4			
Tu	293.8		290	3.8
Tg	301.4	307		5.6
Tg	322.8	320		2.8
Eg	343.6	**356**		**12.4**
Tg	359.1	**348**		**11.1**
Eg	359.2	**374**		**14.8**
Tg	367.1	355		12.1
Tu	369.7		**350**	**19.7**
Ag	370.3	376		5.7
Tu	373.6			
Au	377.5			
Ag	379.8	**397**		**17.2**
Eu	387.0			
Tu	388.4			
Tg	388.4	384		4.4
Tu	396.4			
Eu	400.6			
Ag	407.6	407		0.6
Tu	414.3		410	4.3
Eg	415.6	418		2.4
Tg	420.8	413		7.8
Tu	424.6			
Eg	432.7	432		0.7
Ag	442.5	438		4.5
Au	483.1			

Both optimized geometries agree very well with experimental data. The relative differences between the two geometries are weaker than the 1% typical errors seen in DFT calculations. Then, comparison between computed and measured phonons provides an efficient tool to identify weak symmetry breaking.

Tables I and II show the phonon energies calculated by DFT in the $Pm\bar{3}$ and $P23$ groups, respectively, as well as the best possible assignment for our experimental data in the low

TABLE II. Calculated phonons frequencies in the $P23$ group at 0 K and assignations with the experimental data in the low temperature phase at 9 K. Modes highlighted in pink are both IR and Raman active at low temperature.

Calculations $P23$ (0 K)		Experiments Raman	IR [29]	Comparison error
Irr. Rep.		ν (cm^{-1})		
T	0			
T	75.5		75	0.5
T	88.9		85	3.9
T	132.7			
A	152.5			
T	159.3	165		5.7
A	161.7	**162**		**0.3**
T	184.0		190	6
T	206.4			
E	207.2			
T	211.6		210	1.6
T	224.2	**225**	220	**0.8**
E	237.6			
T	238.4		230	8.4
T	243.4	244		0.6
T	258.6		255	3.8
T	279.3			
T	294.0		290	4
T	301.0	307		6
T	323.3	320		6.7
E	342.3			
T	358.6	**348**	**350**	**8.6**
E	359.8	**356**		**3.8**
T	366.6	355		11
A	369.0			
T	369.3			
T	372.9			
A	377.1	376		1.1
A	382.4	**397**		**14.6**
E	386.8	**374**		**12.8**
T	388.2	384		4.2
T	389.3			
T	397.5			
E	399.6			
A	408.7	407		1.7
T	414.7	413	410	1.7
E	416.4	418		1.6
T	421.5			
T	424.9			
E	433.8	432		1.8
A	443.6	438		5.6
A	475.6			

temperature phase. Symmetry analysis yields to the following decomposition into the irreducible representations of the $Pm\bar{3}$ group:

$$\overbrace{1T_u}^{\text{Accoustic}} \oplus \overbrace{14T_u \oplus 3E_u \oplus 3A_u \oplus 11T_g \oplus 5E_g \oplus 5A_g}^{\text{Optic}},$$

so there are a total of 21 Raman active modes.

And the $P23$ group,

$$\overbrace{1T}^{\text{Accoustic}} \oplus \overbrace{25T \oplus 8E \oplus 8A}^{\text{Optic}},$$

so there are a total of 42 modes.

The measured phonon modes have been assigned to the calculated phonon modes with respect to their symmetries and energies. In the $Pm\bar{3}$ space group, a significant discrepancy between the experimental results and the theoretical calculations is observed for three modes, namely the A_g mode at 397 cm^{-1}, the T_g mode at 225 cm^{-1}, and the T_u mode at 350 cm^{-1}. Especially, it is worth noting that in the $Pm\bar{3}$ space group, there is no other calculated T_g or T_u modes close enough in energy that could be assigned to the observed T_g mode at 225 cm^{-1} and to the T_u mode at 350 cm^{-1}, thus rolling out any assignments ambiguity. If one lifts the inversion center symmetry of the $Pm\bar{3}$ space group and consider the $P23$ space group, the three modes T_g (225 cm^{-1}), A_g (397 cm^{-1}), and T_u (350 cm^{-1}) can be assigned to the calculations with a substantially reduced error (cf. Table II). Moreover, the energy error on the modes at 162 cm^{-1}, 348 cm^{-1}, 356 cm^{-1}, and 374 cm^{-1} is also reduced (cf. Table II).

An additional evidence of the loss of inversion symmetry is provided by the comparison between Raman and IR activity [29]. Indeed, three sets of phonons at 225, 348, and 410 cm^{-1} are both IR and Raman active at low temperature (highlighted in pink in Table II). This is only possible if a breaking of inversion center symmetry happens. More precisely, in the low temperature phase, the modes at 225 and 348 cm^{-1} become Raman active while the mode at 410 cm^{-1} becomes IR active thanks to the loss of inversion symmetry. Based on these observations, we can conclude that the space group $P23$ better describes the low temperature phase than the $Pm\bar{3}$ space group.

IV. LATTICE DYNAMICS OF THE METALLIC PHASE AT HIGH TEMPERATURE

Figure 4 presents the Raman spectra of $PrRu_4P_{12}$ at 300 K for all symmetries. As previously reported [27,30], we detect all eight phonons expected in the $Im\bar{3}$ space group of $PrRu_4P_{12}$, i.e., $2\,E_g + 4\,T_g + 2\,A_g$. In this work, thanks to an improved signal to noise ratio, two additional phonons are measured at 171 cm^{-1} and 331 cm^{-1}, respectively [Cf. Fig. 4(b)], directly questioning the space group assignment to $Im\bar{3}$. As shown in the inset of Fig. 4(b), the mode at 171 cm^{-1} sets on a large mode (FWHM $\sim$15 cm^{-1}), attributed to the crystal-field excitation of the Pr ions as shown by previous temperature-dependent measurements [31]. The mode at 171 cm^{-1} is narrower than the crystal-field mode. As shown in the inset, it also remains similar in shape and position at intermediate temperature above the transition, contrary to the crystal-field excitation on which it sets. It clearly distinguished it from crystal-field excitations. The mode at 331 cm^{-1}, measured in the $A_g + E_g$ and $A_g + E_g + T_g$ configurations (Cf. Fig. 4), is quite narrow with a FWHM of 3.8 cm^{-1} . Its temperature evolution points to a hardening when cooling down from room temperature. Below 80 K, it is not possible to single it out from the E_g high intensity mode at $\sim$370 cm^{-1} . The behavior of both modes, together to

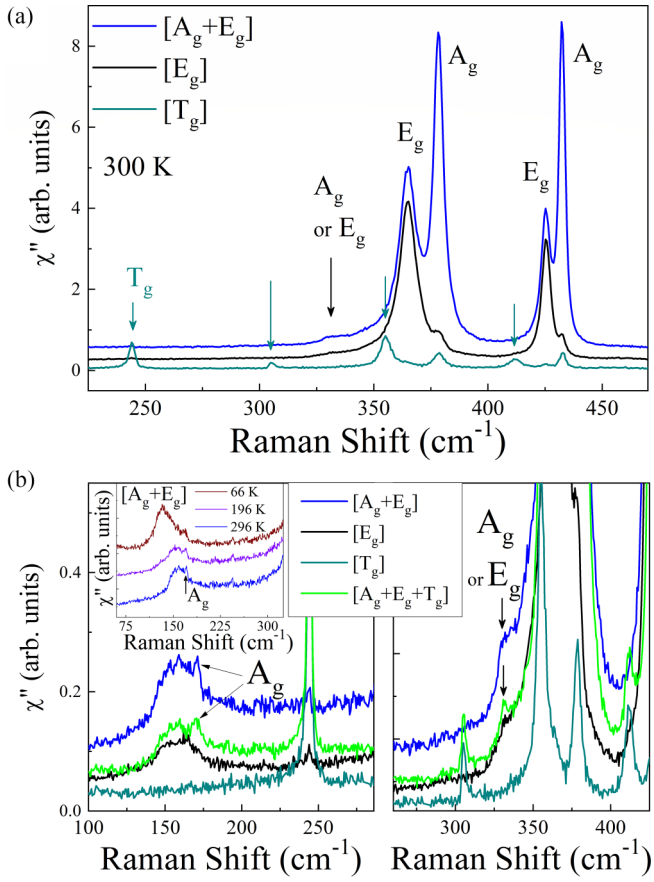

FIG. 4. Raman susceptibility of $PrRu_4P_{12}$ at 300 K in $A_g + E_g$, in the pure E_g, in the pure T_g, and in the $A_g + E_g + T_g$ symmetries. (a) Green arrows indicate the T_g phonon modes and the black arrow indicates a A_g or E_g phonon mode. (b) Zooms on the Raman susceptibility of $PrRu_4P_{12}$ at 300 K showing the phonons at 171 cm^{-1} and 331 cm^{-1} unattributed in the $Im\bar{3}$ space group. Inset: Focus on the A_g mode in the $A_g + E_g$ configuration at intermediate temperature in the metallic state.

the high temperature state of this compound (simple metallic without magnetic or orbital ordering) point to their phononic nature. Below 60 K, moreover, two additional broad modes are observed at 100 cm^{-1} and 40 cm^{-1} in the T_g and $A_g + E_g$ symmetries, respectively. Both are interpreted as crystal-field excitations.

Experimental phonon energies at 300 K, obtained by our Raman spectroscopy experiment and by optical conductivity measurements data taken from the literature [29], are reported in Table III with their best possible assignment to our calculations in the $Im\bar{3}$ space group. The optimized structure is in very good agreement with the experimental data, with a unit cell parameter of 8.0714 Å (exp. 8.0420 Å), $y_P = 0.1448$, and $z_P = 0.3572$ (exp. 0.142 and 0.359).

Both new phonon modes observed at 171 cm^{-1} and 331 cm^{-1}, respectively, cannot be assigned in the $Im\bar{3}$ space group. Indeed, only two A_g optical modes are expected in this space group while the experimental data clearly shows at least three optical A_g modes, and eventually one more if we consider the undetermined A_g or E_g mode at 331 cm^{-1} . Furthermore, the errors between experimental and computed values are very large (43 cm^{-1} and 85 cm^{-1}, respectively) for the A_g modes, far over standard DFT errors on phonons frequencies (typically, 10 to 15 cm^{-1}). Therefore, it seems that the $Im\bar{3}$ space group assigned, up to now, to the crystal structure of $PrRu_4P_{12}$ at high temperature is questionable [11].

TABLE III. Calculated phonons frequencies in the $Im\bar{3}$ group at 300 K and assignments to the experimental data at 300 K. Bottom: Phonons that cannot be assigned in the $Im\bar{3}$ space group.

Calculations $Im\bar{3}$ (300 K)		Experiments (300 K) Raman	IR[29]	Comparison error
Irr. Rep.		ν (cm^{-1})		
Tu	0			
Tu	88.1			
Au	160.8			
Tu	183.0			
Eu	206.5			
Tu	211.3			
Tg	241.7	246		4.3
Tu	257.5		255	2.5
Tu	293.1		290	3.1
Tg	301.8	309		7.2
Eg	353.4	368		14.6
Tg	362.4	359		3.4
Tu	368.5		350	18.5
Au	376.1			
Tu	393.8			
Eu	398.4			
Tu	423.6			
Ag	425.5	**382**		**43.5**
Tg	429.0	412		17
Eg	437.2	430		7.2
Ag	520.7	**436**		**84.7**
		Unassigned modes		
Ag		171		
Ag or Eg		331		

In the following, we will look for new space groups (rather than $Im\bar{3}$) that could reproduce all the Raman modes observed. Since the $P23$ space group has been asserted for the low temperature phase, a supergroup of $P23$ is a good candidate. According to the Bilbao crystallographic server [32], the $P23$ supergroups are $Pn\bar{3}m$, $Pm\bar{3}n$, $Pn\bar{3}n$, $Pm\bar{3}m$, $P\bar{4}3n$, $P\bar{4}3m$, $P4232$, $P432$, $Pn\bar{3}$, $Pm\bar{3}$, $I23$, $Im\bar{3}m$, $I\bar{4}3m$, $I432$, and $Im\bar{3}$.

The systematic symmetry analysis of the Wyckoff sites splitting, and of the irreducible representations of the phonons, allowed us to reduce our candidates to the ones compatible with the experimental data. At room temperature, one sees in Raman scattering experiments three or four A_g modes, two or three E_g modes, four T_g modes, and in IR three potentially "ungerade" modes. Therefore, amongst the $P23$ supergroups, only three of them can produce the desired phonon modes:

$I23$: $13T \oplus 4E \oplus 4A_u$,
$Pm\bar{3}$: $15T_u \oplus 3E_u \oplus 3A_u \oplus 11T_g \oplus 5E_g \oplus 5A_g$,
$P23$: $26T \oplus 8E \oplus 8A$.

TABLE IV. Calculated phonons frequencies in the I23 group and assignments to the experimental data at 300 K. Bottom: Phonons that cannot be assigned in the I23 space group.

Calculations I23 (300 K)		Experiments (300 K) Raman	IR[29]	Comparison error
Irr. Rep.		ν (cm^{-1})		
T	0			
T	87.0			
A	157.4			
T	181.6			
E	207.2			
T	212.0			
T	223.1	246		22.9
T	258.3		255	3.3
T	292.8		290	2.8
T	302.9	309		6.1
E	357.9	368		10.1
T	358.3		350	8.3
T	369.8	359		10.8
A	372.6	382		9.4
T	394.6			
A	397.8			
E	400.0			
T	422.4	412		10.4
E	432.6	430		2.6
A	433.2	436		2.8
T	453.8			
		unassigned modes		
A		171		
A or E		331		

We performed DFT geometry optimization and phonon calculations for these three groups using an electronic temperature of 300 K. It is worth noting that among these groups only $I23$ is compatible with the structural modulation of vector $\mathbf{q} = (100)$, associated with the metal-insulator phase transition [16]. Indeed, in the other groups the two Pr sites are symmetry independent. Tables IV, V, and VI report the computed phonons in the $I23$, $Pm\overline{3}$, and $P23$ groups at 300 K, as well as the best assignment with our experimental Raman data and with the IR data [29]. It appears clearly that two phonon modes could not be assigned in the $I23$ group, namely the A_g mode at 171 cm^{-1} and the A_g (or eventually E) mode at 331 cm^{-1}. The $I23$ space group is thus unsuitable to describe the high temperature phase of the $PrRu_4P_{12}$ compound. In contrast, with the space group $Pm\overline{3}$ and its subgroup $P23$, we can assign all the observed phonon modes with the calculated ones in the right symmetries. Moreover, the error on the energies between experiment and theory is found to be low. Thus, we conclude that the high temperature phase in the $PrRu_4P_{12}$ compound is most likely $Pm\overline{3}$, the most symmetric one, and below T_{MI}, a structural transition occurs to $P23$.

The assignment to the $Pm\overline{3}$ space group at room temperature appears to be compatible with early x-ray powder diffraction experiments [11]. Indeed, $Pm\overline{3}$ and $Im\overline{3}$ space groups are expected to give identical x-ray powder diffraction profiles, i.e., the same reflections with identical intensities.

TABLE V. Calculated phonons frequencies in the Pm$\overline{3}$ group and assignations with the experimental data in the high temperature phase.

Calculations Pm$\overline{3}$ (300 K)		Experiments (300 K) Raman	IR[29]	Comparison error
Irr. Rep.		ν (cm^{-1})		
Tu	0			
Tu	72.9			
Tu	88.3			
Tg	132.7			
Tg	159.3			
Au	161.7			
Ag	174.1	171		3.1
Tu	183.8			
Tg	206.9			
Eu	207.0			
Tu	212.0			
Tu	224.0			
Tu	235.5			
Eg	241.6			
Tg	242.6	246		3.4
Tu	258.3		255	3.3
Tg	279.4			
Tu	293.9		290	3.9
Tg	301.1	309		
Tg	322.1			
Eg	348.0	331		14
Eg	359.2	368		8.8
Tg	359.3	359		0.3
Tg	366.9			
Tu	369.0		348	21
Tu	372.5			
Ag	376.7			
Au	377.3			
Ag	379.6	382		2.4
Eu	387.1			
Tg	388.6			
Tu	389.4			
Tu	395.1			
Eu	399.9			
Ag	408.9			
Tu	411.9			
Eg	419.8			
Tg	422.0	412		10
Tu	423.7			
Eg	431.2	430		1.2
Ag	440.8	436		4.8
Au	482.6			

V. DISCUSSION

The structural phase transition from $Pm\overline{3}$ to $P23$ preserves the Pr atoms position (Wyckoff position 1a and 1b). At room temperature, in the $Pm\overline{3}$, the Ru and P cages have the same shape at both Pr sites but different volumes. The main effect through the transition obtained by our calculations relies in the change of the size of the Ru and P cages. In principle both cages could be distorted from $Pm\overline{3}$ to $P23$ as the Ru atoms have two different sites and the phosphorus atoms are both in

TABLE VI. Calculated phonons frequencies in the P23 group and assignations with the experimental data in the high temperature phase.

Calculations P23 (300 K)		Experiments (300 K) Raman	IR[29]	Comparison error
Irr. Rep.		ν (cm^{-1})		
T	0			
T	74.5			
T	88.9			
T	132.7			
T	159.2			
A	161.6			
A	174.2	171		3.2
T	184.0			
T	206.9			
E	207.0			
T	212.0			
T	224.0			
T	236.3			
E	241.7			
T	243.1	246		2.9
T	258.3		255	3.3
T	279.5			
T	293.8		290	3.8
T	301.2	309		7.8
T	322.0			
E	347.8	331		16.8
E	359.6	368		8.4
T	359.7		348	11.7
T	366.2	359		7.2
T	369.7			
T	372.7			
A	376.9			
A	377.3			
A	380.7	382		1.3
E	387.3			
T	388.2			
T	390.1			
T	395.4			
E	399.3			
A	409.4			
T	412.7	412		0.7
E	420.6			
T	423.2			
T	424.0			
E	431.4	430		1.4
A	441.1	436		5.1
A	478.5			

the 12j Wyckoff position in the low temperature phase. Nevertheless, the distortions we obtained are of the order of 10^{-7} of the lattice parameter and are then below the significance of our calculations.

As illustrated in Fig. 3(b), the phosporus cages become more similar in volume when crossing the transition into $P23$ while the one on Pr(1) atoms becomes larger than the one on Pr(2). On the contrary, the Ru cages keep the same tendency in volume, i.e., the Ru cages on Pr(1) is always larger than on Pr(2) and this tendency is reinforced when entering the $P23$ phase consistently to what was extracted by Lee *et al.* [16]. Quantitatively, they report a change of volume of the Ru cages, where Pr(1)-Ru and Pr(2)-Ru bond lengths are 3.490(3) and 3.470(3) Å (i.e., a difference of 0.02 Å) while we obtained in the $P23$ space group that Pr(1)Ru =3.501 Å and Pr(2)Ru=3.490 Å (i.e., a difference of 0.011 Å). Besides, from EXAFS measurements, Cao *et al.* [19] report that the Ru-Ru distances on both cages are separated by about 0.022–0.030 Å, and we obtained a difference on the Ru-Ru distances of 0.013 Å. All these values are reasonable and support the main tendencies. As for the P cages, Lee *et al.* [16] report that the bond lengths Pr(1)P(1) and Pr(2)P(2) are equivalent at low temperature [3.100(3) Å] while we calculate Pr(1)P(1)=3.11058 and Pr(2)P(2)=3.11049. Our difference between bond distances is very small ($\sim 10^{-4}$) and beyond the expected accuracy of both calculations and measurements.

Interestingly, in both the $Pm\bar{3}$ and $P23$ groups the two Pr sites are independent, contrarily to the $Im\bar{3}$ group were the two Pr sites are symmetry related. Additionally, the loss of the inversion center occurs on the Pr sites at the T_{MI} transition. The crystal field levels, their irreducible representations, number, and degeneracy on each Pr site are, however, the same for both space groups, as in the $Im\bar{3}$ group. More precisely, the crystal field levels remain: one singlet Γ_1, two triplets Γ_4, and a doublet Γ_{23}. Pr XANES measurements indicate that the Pr atoms are trivalent, in the whole temperature range between 20 K and 300 K, i.e., through the transition [33]. There are then two electrons per Pr ions. Considering the one-electron orbitals on the Pr^{3+} ions, the interesting consequence of the loss of inversion center is the new possibility of hybridization between the one-electron orbitals of the Pr ions. Indeed, in $P23$ the one-electron $4f$ orbitals belonging to the Γ_4 (T) irreducible representation are allowed to hybridize with the ($5d_{xy}$, $5d_{xz}$, $5d_{yz}$) triply degenerated (also T) orbitals. In the $Pm\bar{3}$ group, the $4f$ orbitals belong to Γ_4^- (T_u), and the $5d$ orbitals to Γ_4^+ (T_g) and thus, they cannot hybridize. Similarly, in $P23$ the Γ_1 (A) one-electron $4f$ orbital $F_{-2} = xyz$, is allowed to hybridize with the $6s$ one, while in $Pm\bar{3}$ they respectively belong to Γ_1^- (A_u) and Γ_1^+ (A_g). The $4f$ spatial extension of the $4f$ orbitals is thus expected to be wider in the low-symmetry $P23$ group.

As a result, since $PrRu_4P_{12}$ belongs to the noncentrosymmetric group at low temperature, the delocalization of the $4f$ two-electron states is enhanced in this phase, and the hybridization with the conduction electrons from the Ru-$4d$ orbitals and/or P-$3p$ orbitals is expected to be facilitated when crossing the transition to lower temperature. RIXS study [14] reports that the contribution of the Ru-$4d$ electronic state to the ordered phase is probably negligible, pointing to a main effect rather than coming from the $3p$ electrons of the P. Theoretical work [10,34] supports the idea of a Γ_4 ground state on the Pr(1) site stabilized by the intermediate $4f^3$ state, while the Pr(2) will have a $4f^1$ character in the Γ_1 CEF state. It is worth noting that our calculations point to a shrinking of the P cages on the Pr(2) ions at low temperature. Being in the Γ_1 ground state, the $4f$ electrons on the Pr(2) ions would indeed be more delocalized toward a tendency to the $4f^1$ intermediate state. To summarize, the loss of inversion center in $P23$ space group has an impact on the hybridization between the $4f$ and

the *Ru* and *P* electrons; thus it may be an important ingredient to be considered to unveil the nature of the low temperature phase ordering.

VI. CONCLUSION

The filled skutterudite $PrRu_4P_{12}$ was investigated by Raman scattering measurements and DFT calculations. We strongly question the previously reported $Im\bar{3}$ room temperature crystal structure and identify it as $Pm\bar{3}$, i.e., with two distinct Pr sites. The low temperature space group is consistently described to be $P23$, i.e., noncentrosymmetric. While the crystal field levels scheme (symmetry and degeneracy) is the same in these three space groups, the main consequence of the transition from $Pm\bar{3}$ to $P23$ is to facilitate hybridization between the $4f$ electrons of the Pr with Ru and P electrons.

ACKNOWLEDGMENTS

This work was supported by the French Agence Nationale de la Recherche (ANR SEO-HiggS2, Grant No. ANR-16-CE30-0014). The calculations presented in this work were performed on the IDRIS French computer center under Project No. 0801842, and on the CRIANN Normandie computer center under Project No. 2007013.

[1] G. Mahan, B. Sales, and J. Sharp, Thermoelectric materials: new approaches to an old problem, Phys. Today **50**(3), 42 (1997).

[2] Y. Aoki, H. Sugawara, H. Hisatomo, and H. Sato, Novel kondo behaviors realized in the filled skutterudite structure, J. Phys. Soc. Jpn. **74**, 209 (2005).

[3] H. Sato, D. Kikuchi, K. Tanaka, M. Ueda, H. Aoki, T. Ikeno, S. Tatsuoka, K. Kuwahara, Y. Aoki, M. Kohgi *et al.*, Novel features realized in the filled skutterudite structure, J. Phys. Soc. Jpn. **77**, 1 (2008).

[4] H. Sato, D. Kikuchi, K. Tanaka, H. Aoki, K. Kuwahara, Y. Aoki, M. Kohgi, H. Sugawara, and K. Iwasa, Novel electronic states realized in the filled skutterudites containing rare earth elements with more than one $4f$-electrons, J. Magn. Magn. Mater. **310**, 188 (2007).

[5] E. D. Bauer, N. A. Frederick, P.-C. Ho, V. S. Zapf, and M. B. Maple, Superconductivity and heavy fermion behavior in $PrRu_4P_{12}$, Phys. Rev. B **65**, 100506(R) (2002).

[6] M.-A. Measson, D. Braithwaite, J. Flouquet, G. Seyfarth, J. P. Brison, E. Lhotel, C. Paulsen, H. Sugawara, and H. Sato, Superconducting phase diagram of the filled skuterrudite $PrRu_4P_{12}$, Phys. Rev. B **70**, 064516 (2004).

[7] M. B. Maple, N. P. Butch, N. A. Frederick, P.-C. Ho, J. R. Jeffries, T. A. Sayles, T. Yanagisawa, W. M. Yuhasz, S. Chi, H. J. Kang *et al.*, Field-dependent ordered phases and kondo phenomena in the filled skutterudite compound $PrOs_4As_{12}$, Proc. Natl. Acad. Sci. USA **103**, 6783 (2006).

[8] Y. Aoki, T. Tayama, T. Sakakibara, K. Kuwahara, K. Iwasa, M. Kohgi, W. Higemoto, D. E. MacLaughlin, H. Sugawara, and H. Sato, The unconventional superconductivity of skutterudite $PrOs_4Sb_{12}$: Time-reversal symmetry breaking and adjacent field-induced quadrupole ordering, J. Phys. Soc. Jpn. **76**, 051006 (2007).

[9] K. Kuwahara, K. Iwasa, M. Kohgi, K. Kaneko, N. Metoki, S. Raymond, M.-A. Measson, J. Flouquet, H. Sugawara, Y. Aoki, and H. Sato, Direct observation of quadrupolar excitons in the heavy-fermion superconductor $PrRu_4P_{12}$, Phys. Rev. Lett. **95**, 107003 (2005).

[10] J. Otsuki, H. Kusunose, and Y. Kuramoto, Theory of crystalline electric field and kondo effect in Pr skutterudites, J. Phys. Soc. Jpn. **74**, 200 (2005).

[11] C. Sekine, T. Uchiumi, I. Shirotani, and T. Yagi, Metal-insulator transition in $PrRu_4P_{12}$ with skutterudite structure, Phys. Rev. Lett. **79**, 3218 (1997).

[12] K. Iwasa, L. Hao, K. Kuwahara, M. Kohgi, S. R. Saha, H. Sugawara, Y. Aoki, H. Sato, T. Tayama, and T. Sakakibara, Evolution of $4f$ electron states in the metal-insulator transition of $PrRu_4P_{12}$, Phys. Rev. B **72**, 024414 (2005).

[13] Y. Nakanishi, T. Kumagai, O. Masafumi, T. Tanizawa, and M. Yoshizawa, Ultrasonic study of the filled skutterudite compound $PrRu_4P_{12}$, Phys. Rev. B **73**, 165115 (2006).

[14] H. Nakao and K. Iwasa, Direct observation of modulation of p–f hybridization in unconventional ordered phase of $PrRu_4P_{12}$, J. Phys. Soc. Jpn. **89**, 063703 (2020).

[15] C. H. Lee, H. Matsuhata, A. Yamamoto, T. Ohta, H. Takazawa, K. Ueno, C. Sekine, I. Shirotani, and T. Hirayama, Structural phase transition accompanied by metal-insulator transition in $PrRu_4P_{12}$, J. Phys.: Condens. Matter **13**, L45 (2001).

[16] C. H. Lee, H. Matsuhata, H. Yamaguchi, C. Sekine, K. Kihou, T. Suzuki, T. Noro, and I. Shirotani, Charge-density-wave ordering in the metal-insulator transition compound $PrRu_4P_{12}$, Phys. Rev. B **70**, 153105 (2004).

[17] C. H. Lee, H. Matsuhata, H. Yamaguchi, C. Sekine, K. Kihou, and I. Shirotani, A study of the crystal structure at low temperature in the metal–insulator transition compound $PrRu_4P_{12}$, J. Magn. Magn. Mater. **272-276**, 426 (2004).

[18] L. Hao, K. Iwasa, K. Kuwahara, M. Kohgi, S. R. Saha, H. Sugawara, Y. Aoki, H. Sato, C. Sekine, C. H. Lee, and H. Harima, Crystal-lattice modulation of the metal–insulator transition system $PrRu_4P_{12}$ studied by x-ray diffraction, J. Magn. Magn. Mater. **272-276**, E271 (2004).

[19] D. Cao, R. H. Heffner, F. Bridges, I.-K. Jeong, E. D. Bauer, W. M. Yuhasz, and M. B. Maple, Local distortion induced metal-to-insulator phase transition in $PrRu_4P_{12}$, Phys. Rev. Lett. **94**, 036403 (2005).

[20] S. R. Saha, H. Sugawara, T. Namiki, Y. Aoki, and H. Sato, Anomalous properties in the low-carrier ordered phase of $PrRu_4P_{12}$: Consequence of hybridization between conduction and Pr $4f$ electrons, Phys. Rev. B **80**, 014433 (2009).

[21] R. Dovesi, A. Erba, R. Orlando, C. M. Zicovich-Wilson, B. Civalleri, L. Maschio, M. Rérat, S. Casassa, J. Baima, S. Salustro, and B. Kirtman, Quantum-mechanical condensed matter simulations with CRYSTAL, WIREs Comput Mol Sci **8**, e1360 (2018).

[22] C. M. Zicovich-Wilson, F. Pascale, C. Roetti, V. R. Saunders, R. Orlando, and R. Dovesi, Calculation of the vibration frequencies of α-quartz: The effect of Hamiltonian and basis set, J. Comput. Chem. **25**, 1873 (2004).

[23] J. P. Perdew, A. Ruzsinszky, G. I. Csonka, O. A. Vydrov, G. E. Scuseria, L. A. Constantin, X. Zhou, and K. Burke, Restoring the density-gradient expansion for exchange in solids and surfaces, Phys. Rev. Lett. **100**, 136406 (2008).

[24] M. F. Peintinger, D. V. Oliveira, and T. Bredow, Consistent gaussian basis sets of triple-zeta valence with polarization quality for solid-state calculations, J. Comput. Chem. **34**, 451 (2013).

[25] K. A. Peterson, D. Figgen, M. Dolg, and H. Stoll, Energy-consistent relativistic pseudopotentials and correlation consistent basis sets for the 4*d* elements Y–Pd, J. Chem. Phys. **126**, 124101 (2007).

[26] M. Dolg, H. Stoll, and H. Preuss, Energy-adjusted *ab initio* pseudopotentials for the rare earth elements, J. Chem. Phys. **90**, 1730 (1989).

[27] N. Ogita, R. Kojima, T. Hasegawa, M. Udagawa, H. Sugawara, and H. Sato, Crystal field excitations of filled skutterudite $PrRu_4P_{12}$ by Raman scattering, J. Phys.: Conf. Ser. **150**, 042147 (2009).

[28] K. Momma and F. Izumi, VESTA 3 for three-dimensional visualization of crystal, volumetric and morphology data, J Appl Crystallogr **44**, 1272 (2011).

[29] M. Matsunami, L. Chen, M. Takimoto, H. Okamura, T. Nanba, C. Sekine, and I. Shirotani, Metal-insulator transition in $PrRu_4P_{12}$ and $SmRu_4P_{12}$ investigated by optical spectroscopy, Phys. Rev. B **72**, 073105 (2005).

[30] N. Ogita, K. Yamamoto, S. R. Saha, H. Sugawara, H. Sato, C. Sekine, I. Shirotani, and M. Udagawa, Raman scattering study of filled skutterudite, Phys. B: Condens. Matter **359-361**, 847 (2005).

[31] N. Ogita, R. Kojima, Y. Takasu, T. Hasegawa, T. Kondo, M. Udagawa, N. Takeda, T. Ikeno, K. Ishikawa, H. Sugawara *et al.*, Raman scattering study of the skutterudite compounds, J. Magn. Magn. Mater. **310**, 948 (2007).

[32] M. I. Aroyo, J. M. Perez-Mato, C. Capillas, E. Kroumova, S. Ivantchev, G. Madariaga, A. Kirov, and H. Wondratschek, Bilbao crystallographic server: I. Databases and crystallographic computing programs, Z. Kristallogr. - Cryst. Mater. **221**, 15 (2006).

[33] C. H. Lee, H. Oyanagi, C. Sekine, I. Shirotani, and M. Ishii, XANES study of rare-earth valency in LRu_4P_{12} (L = Ce and Pr), Phys. Rev. B **60**, 13253 (1999).

[34] R. Shiina and H. Shiba, Effective Hamiltonian for $PrRu_4P_{12}$ showing unconventional charge ordering, J. Phys. Soc. Jpn. **79**, 044704 (2010).